Key Points:
- Chlorophyll *a* concentration is retrieved from fluorescence profiles
- Phytoplankton communities size indices are retrieved from fluorescence profiles
- A neural network is developed with a potential for global-scale applications

Correspondence to:
R. Sauzède,
sauzede@obs-vlfr.fr

Retrieving the vertical distribution of chlorophyll a concentration and phytoplankton community composition from in situ fluorescence profiles: A method based on a neural network with potential for global-scale applications

R. Sauzède[1,2], H. Claustre[1,2], C. Jamet[3], J. Uitz[1,2], J. Ras[1,2], A. Mignot[4], and F. D'Ortenzio[1,2]

[1]Laboratoire d'Océanographie de Villefranche, CNRS, UMR7093, Villefranche-Sur-Mer, France, [2]Université Pierre et Marie Curie-Paris 6, UMR7093, Laboratoire d'océanographie de Villefranche, Villefranche-Sur-Mer, France, [3]Laboratoire d'Océanologie et de Géosciences, UMR8187, ULCO/CNRS, Wimereux, France, [4]Department of Earth, Atmospheric and Planetary Sciences, Massachusetts Institute of Technology, Cambridge, Massachusetts, USA

Abstract A neural network-based method is developed to assess the vertical distribution of (1) chlorophyll *a* concentration ([Chl]) and (2) phytoplankton community size indices (i.e., microphytoplankton, nanophytoplankton, and picophytoplankton) from in situ vertical profiles of chlorophyll fluorescence. This method (FLA-VOR for Fluorescence to Algal communities Vertical distribution in the Oceanic Realm) uses as input only the shape of the fluorescence profile associated with its acquisition date and geo-location. The neural network is trained and validated using a large database including 896 concomitant in situ vertical profiles of High-Performance Liquid Chromatography (HPLC) pigments and fluorescence. These profiles were collected during 22 oceanographic cruises representative of the global ocean in terms of trophic and oceanographic conditions, making our method applicable to most oceanic waters. FLAVOR is validated with respect to the retrieval of both [Chl] and phytoplankton size indices using an independent in situ data set and appears to be relatively robust spatially and temporally. To illustrate the potential of the method, we applied it to in situ measurements of the BATS (Bermuda Atlantic Time Series Study) site and produce monthly climatologies of [Chl] and associated phytoplankton size indices. The resulting climatologies appear very promising compared to climatologies based on available in situ HPLC data. With the increasing availability of spatially and temporally well-resolved data sets of chlorophyll fluorescence, one possible global-scale application of FLAVOR could be to develop 3-D and even 4-D climatologies of [Chl] and associated composition of phytoplankton communities. The Matlab and R codes of the proposed algorithm are provided as supporting information.

1. Introduction

Phytoplankton is an essential component in marine biogeochemical cycles and ecosystems. The assessment of its spatio-temporal distribution and variability across the global ocean is thus an important objective in biological oceanography. Methods have been developed for monitoring oceanic phytoplankton distribution (horizontally and vertically) with the objective to continuously increase the spatio-temporal resolution of data acquisition. These methods often rely on the estimation of the chlorophyll *a* concentration which is a universal proxy for phytoplankton biomass. Remote sensing of Ocean Color Radiometry (OCR) offers a unique way to map quasi-synoptically chlorophyll *a* concentration at the ocean surface. Through this technique, a wide range of applications has been developed, leading to a better understanding of phytoplankton dynamics in the upper ocean [*McClain*, 2009; *Siegel et al.*, 2013]. However, the use of remote sensing of OCR provides chlorophyll *a* concentration only for the surface layers of the ocean [*Gordon and McCluney*, 1975], representing one-fifth of the so-called euphotic layer where phytoplankton photosynthesis takes place [*Morel and Berthon*, 1989]. The vertical distribution of phytoplankton thus escapes from this remote detection. While in situ vertical profiles of chlorophyll *a* concentration are determined with the best accuracy by high-performance liquid chromatography (HPLC) [*Claustre et al.*, 2004; *Peloquin et al.*, 2013], this method is not compatible with highly repetitive measurements.

Introduced by *Lorenzen* [1966], measurement of in vivo fluorescence of chlorophyll *a* is a nonintrusive technique that allows the direct in situ assessment of chlorophyll *a* concentration. Besides the dissolved oxygen,

chlorophyll *a* fluorescence is certainly the most measured biogeochemical property in the global ocean. The in vivo fluorescence of chlorophyll *a* can be considered as a proxy for chlorophyll *a* concentration with some unavoidable limitations such as the variability of the fluorescence-to-chlorophyll *a* concentration ratio as a function of physiological constraints or community composition [*Kiefer*, 1973; *Falkowski et al.*, 1985; *Cunningham*, 1996]. While in vivo fluorescence is an imperfect proxy, it presents the advantage that it can be easily measured thanks to miniature in situ sensors. Thus, the inherent weaknesses of fluorometric measurements are largely compensated by their cost effective acquisition that enables numerous data to be gathered. This is now especially true considering that, besides oceanic cruises, in vivo fluorescence is accessible through autonomous platforms (floats, gliders, animals), allowing a global fluorescence database to be progressively assembled [*Claustre et al.*, 2010a, 2010b].

On a case-by-case basis (e.g., an oceanographic cruise), a fluorescence database can be easily and accurately converted into a chlorophyll *a* concentration database, for example, thanks to simultaneous HPLC determination [*Claustre et al.*, 1999]. However, with the goal of developing large-scale chlorophyll *a* concentration databases from the merging of different fluorescence data from diverse origins (e.g., sensors, platforms), their consistency and interoperability will become a critical issue. First, the expected exponential growth of fluorescence profile acquisition in the near future (more and more autonomous platforms will be deployed) will stimulate regular updates of these "super" databases. Hence, methods have to systematically add new data in a way that does not compromise the reliability and the quality of the existing database. Second, as some platforms (e.g., floats, animals) are not necessarily recovered, the initial sensor calibration, if any, would represent the only reference for the whole acquisition period (sometimes extending over several years). This can represent a bias because these platforms acquire fluorescence profiles in conditions where the phytoplankton communities and their physiological state may have drastically changed in comparison to the conditions prevailing at the time of platform deployment and initial sensor calibration. Robust methods that allow the retrieval of chlorophyll *a* concentration from fluorescence measurements without any regular or simultaneous HPLC measurement will need to be developed.

Several alternative methods have already been proposed for calibrating fluorescence profiles, which partly circumvent the above mentioned issues. *Lavigne et al.* [2012] use the satellite remotely detected surface chlorophyll *a* concentration as a way to scale the whole fluorescence vertical profile to this reference surface value. While this method presents the advantage of allowing the interoperability of data sets from different origins and locations, it is obviously not applicable to situations where no concurrent satellite data are available (SeaWiFS was launched in 1997). Furthermore, it implicitly postulates that the satellite-derived surface chlorophyll *a* concentration is the "accurate" reference, an assumption that can be challenged, especially in some oceanic regions [e.g., *Bricaud et al.*, 2002; *Johnson et al.*, 2013]. *Mignot et al.* [2011] have shown that information related to chlorophyll *a* concentration is embedded in the shape of the fluorescence profile. For example, it is intuitive that the deeper the Deep Chlorophyll maximum (DCM), the lower the surface chlorophyll *a* concentration [see also, *Morel and Bertrhon*, 1989; *Uitz et al.*, 2006]. *Mignot et al.* [2011] thus proposed a calibration of the fluorescence profile based on its shape. The prerequisite of the method is that the profile shape has to be a priori categorized either into a stratified type (modeled by a Gaussian) or a mixed type (modeled by a sigmoid). Clearly, the advantage of this method is that it does not require any complementary information. Its limit lies in the need for an initial classification of the fluorescence profiles, which may be complicated for those that do not clearly belong to one of the two categories.

The primary objective of the present study relies on, and further extends, the approach of *Mignot et al.* [2011]. It aims at developing a self-consistent calibration method of the fluorescence profile essentially based on its shape, and which requires minimum additional information or a priori knowledge. The choice of limiting the use of additional information is essentially guided by the long-term objective of this study, which is to reconcile the oldest databases (assembled during the 1970s when the first fluorescence profiles were recorded with no or scarce ancillary data) with the most recent as well as future databases (derived from autonomous platforms). Besides the fluorescence profile, its geo-location represents robust additional information that is systematically present (as metadata) and potentially useful. At first order (e.g., on a global scale), the geo-location indeed intrinsically embeds information relative to the trophic status (amount of biomass, e.g., spring bloom in the North Atlantic) or hydrographic conditions (stratified versus mixed, e.g., subtropical gyres versus upwellings).
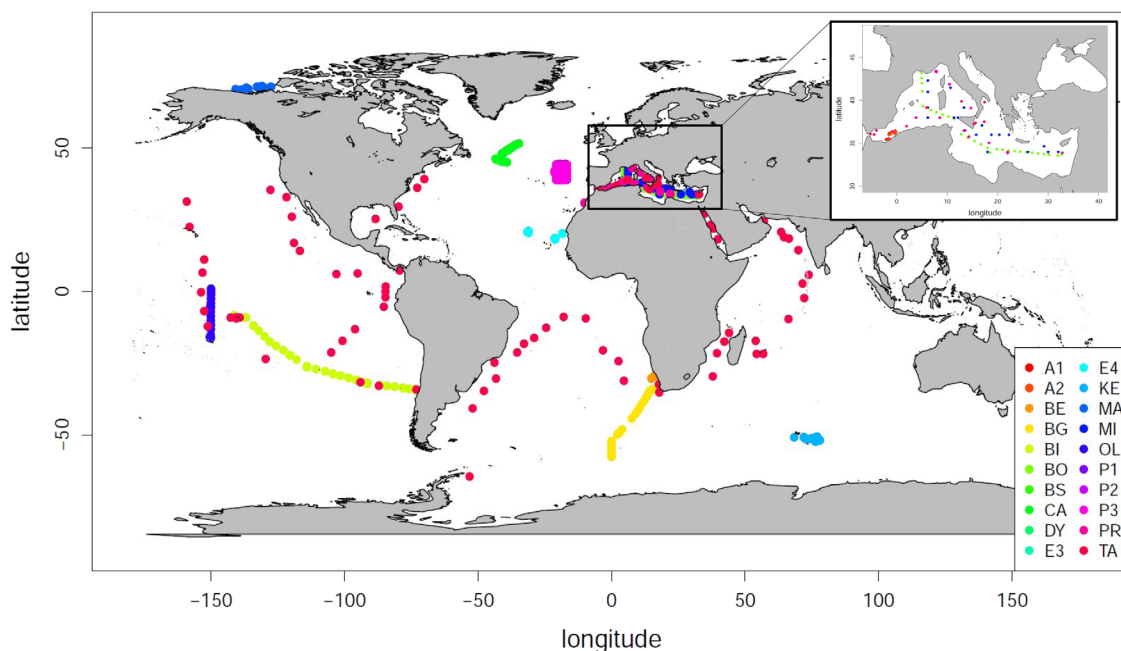
Figure 1. Geographic distribution of the 896 stations used in the present study. For these stations, sampling for HPLC pigment was simultaneous to the acquisition of the fluorescence profile.

Artificial neural networks (ANNs) are approximate functions of any data sets [*Marzban*, 2009]. They represent powerful methods to develop models especially when the underlying relationships are unknown, which is typically the case here with the fluorescence profile shape and the chlorophyll *a* concentration. In particular, multilayered perceptrons (MLPs) are universal approximators of any differentiable and continuous function [*Hornik et al.*, 1989] which are well adapted to ecological data sets having often nonlinear spatially and temporally complex and noisy distributions [*Lek and Guégan*, 1999]. In oceanography, such methods have been developed and used for the retrieval of various products such as the diffuse attenuation coefficient [*Jamet et al.*, 2012], the partial pressure of carbon dioxide (pCO_2) surface distribution [*Friedrich and Oschlies*, 2009; *Telszewski et al.*, 2009], the surface phytoplankton pigment concentration [*Gross et al.*, 2000] or the surface phytoplankton functional types [*Bricaud et al.*, 2007; *Raitsos et al.*, 2008; *Ben Mustapha et al.*, 2013; *Palacz et al.*, 2013]. These methods thus appear well adapted to the type of problem identified here, i.e., the retrieval of a calibrated chlorophyll *a* concentration profile from the shape and geo-location of a fluorescence profile.

In most studies dealing with the possible impact of environmental changes on oceanic carbon fluxes, the nature of phytoplankton communities (e.g., performing regenerated versus new production, small versus large phytoplankton) is an essential variable to account for [e.g., *Le Quere et al.*, 2005]. Ongoing efforts are underway to synthesize the historical knowledge on phytoplankton taxonomy in gathered databases [e.g., *Buitenhuis et al.*, 2012; *Leblanc et al.*, 2012]. These data sets, nevertheless, remain rather sparse and the possibility to regularly improve and update them is weak simply because there are less taxonomic experts than before. Alternative procedures thus need to be developed. *Uitz et al.* [2006] have shown that phytoplankton size indices can be derived from High-Performance Liquid Chromatography (HPLC) pigment analysis [see also *Peloquin et al.*, 2013]. These indices can be related to surface chlorophyll *a* concentration, so that explicit relationships can be observed between the phytoplankton biomass (e.g., chlorophyll *a* concentration), the phytoplankton communities (e.g., phytoplankton size indices) and their vertical distribution.

In summary, the twofold objective of the present study is to retrieve, from the sole knowledge of the fluorescence profile shape and geo-location, the vertical profile of (1) chlorophyll *a* concentration and (2) phytoplankton community size indices. To address this objective, we developed a MLP-based method, hereafter referred to as FLAVOR for Fluorescence to Algal communities Vertical distribution in the Oceanic Realm. The MLP is trained and validated using an in situ database that contains 896 continuous vertical fluorescence

Table 1. Abbreviations Used in the Present Study and Their Significance

Abbreviations	Significance
[TChl]	Chlorophyll a concentration associated to the total phytoplankton biomass (mg m^{-3})
fmicro	Fraction of chlorophyll a associated to microphytoplankton
fnano	Fraction of chlorophyll a associated to nanophytoplankton
fpico	Fraction of chlorophyll a associated to picophytoplankton
[microChl]	Total chlorophyll a concentration associated to microphytoplankton (mg m^{-3})
[nanoChl]	Total chlorophyll a concentration associated to nanophytoplankton (mg m^{-3})
[picoChl]	Total chlorophyll a concentration associated to picophytoplankton (mg m^{-3})
[Chl]	Chlorophyll a concentration (mg m^{-3}) referring either to [TChl] or [microChl], [nanoChl], and [picoChl]
[TChl]$_{Z_0}$	[TChl] integrated from the surface up to the depth Z_0 (mg m^{-2})
z	Geometrical depth (m)
Z_0	Depth at which the fluorescence begins to be constant with depth (m)
Z_e	Euphotic layer depth (m)
Z_m	Mixed layer depth (m)
ζ	Depth normalized with respect to Z_0, $\zeta = z/Z_0$, dimensionless
Fuco	Fucoxanthin (mg m^{-3})
Perid	Peridinin (mg m^{-3})
Hex-fuco	19′-Hexanoyloxyfucoxanthin (mg m^{-3})
But-fuco	19′-Butanoyloxyfucoxanthin (mg m^{-3})
Allo	Alloxanthin (mg m^{-3})
TChl$b$	Chlorophyll b + divinyl Chlorophyll b (mg m^{-3})
Zea	Zeaxanthin (mg m^{-3})
Lon	Longitude (°E)
Day	Day of the year
Lon$_{rad}$	Longitude transformed in radians
Day$_{rad}$	Day transformed in radians
fluo	The fluorescence (relative units)
fluo$_{norm}$	The normed fluorescence (dimensionless)
[Chl]$_{HPLC}$	The [Chl] values of reference estimated by HPLC (mg m^{-3})
[Chl]$_{MLP}$	The 10 discrete values of [Chl] returned by the MLP (mg m^{-3})
[Chl]$_{cal}$	The fluorescence profile calibrated in [Chl] (mg m^{-3})
α	The calibration coefficient, such as $[TChl]_{cal} = \alpha \cdot fluo$
MAPD	Median absolute percent difference (%)
a	The slope of the linear regression between [Chl]$_{MLP}$ or [Chl]$_{cal}$ and the reference values of [Chl] estimated by HPLC

profiles acquired simultaneously to HPLC pigment determinations at selected depths. This database is representative of the range of trophic and oceanographic conditions prevailing in the global open ocean. Therefore, we expect that any potential conclusion of the present study will be of general applicability to the global ocean.

2. Data Presentation and Processing

2.1. Database of Vertical Profiles of Chlorophyll Fluorescence and HPLC Pigments

The present study makes use of an extensive database of concurrent vertical profiles of chlorophyll fluorescence (fluo, see abbreviations in Table 1) and phytoplankton pigments determined by HPLC. This data set is an extension of the one used by *Mignot et al.* [2011]. The data were collected at 896 stations sampled during 22 open ocean cruises between 1991 and 2012 (Table 2), which took place in a wide variety of oceanic regions. Most of the data were collected in the Mediterranean Sea (39%) and the Atlantic Ocean (36%), 17% of the data are from the Pacific Ocean, 3% from the South Ocean, 3% from the Arctic Ocean, and 2% from the Indian Ocean (Figure 1).

The chlorophyll a in vivo fluorescence profiles acquired during the 22 cruises were obtained using a fluorometer mounted on a CTD-rosette. We applied a quality control to each fluorescence profile similarly to *D'Ortenzio et al.* [2010] in order to remove aberrant data caused by electronic noise.

Samples for HPLC pigment determinations were acquired at discrete depths (approximately 10 data points per profile) and analyzed according to the method described by *Claustre* [1994] for the EUMELI cruises, *Vidussi et al.* [1996] for the cruises that occurred prior to 2004, and *Ras et al.* [2008] for all other cruises after 2004. The concentration of total chlorophyll a as determined by HPLC actually refers to the concentration of the so-called total chlorophyll a ([TChl]) which is the sum of the concentrations of monovinyl-chlorophyll a, divinyl-chlorophyll a, chlorophyllide a and the allomeric and epimeric forms of chlorophyll a. [TChl] is an estimate of the total phytoplankton biomass. In addition to chlorophyll a, the HPLC technique enables

Table 2. Abbreviations, Location, Period, Number of Stations (After Quality Control) and References or PI for Each Cruises/Projects Used in the Data Set

Cruise/Project	Abbreviation	Location	Period	Number of Stations	References or PI
Almofront1	A1	Alboran Sea	Apr–May 1991	18	Claustre et al. [1994] and Peloquin et al. [2013]
Almofront2	A2	Alboran Sea	Nov 1997–Jan 1998	37	Claustre et al. [2000], Uitz et al. [2006], and Peloquin et al. [2013]
Bencal	BE	Benguela upwelling	Oct 2002	5	Morel et al. [2006] and Peloquin et al. [2013]
Biosope	BI	South Pacific	Austral Summer 2004	60	Ras et al. [2008] and Peloquin et al. [2013]
Bonus Good Hope	BG	Southern Ocean	Feb–Mar 2008	23	PI: Claustre and Ras
Boum	BO	Mediterranean Sea	Jun–Jul 2008	28	Crombet et al. [2011] and Peloquin et al. [2013]
Boussole	BS	7.54°E, 43.22°N	2001–2007	75	PI: Antoine and Ras
CATCH	CA	North Atlantic	Jan–Feb 1997	26	Uitz et al. [2006] and Peloquin et al. [2013]
Dyfamed	DY	7.54°E, 43.22°N	1994–1999	32	Marty et al. [2002] and Peloquin et al. [2013]
Eumeli3	E3	Sub-tropical North Atlantic	Sep–Oct 1991	15	Claustre and Marty [1995] and Peloquin et al. [2013]
Eumeli4	E4	Sub-tropical North Atlantic	May–Jun 1992	22	Claustre and Marty [1995] and Peloquin et al. [2013]
Keops	KE	Southern Ocean	Jan–Feb 2005	16	Uitz et al. [2009]
HUDSON 2013-008	LA	Labrador Sea	May 2013	22	PI: Claustre and Ras
Malina	MA	Arctic Ocean	Jul–Nov 2009	24	Huot et al. [2013]
Minos	MI	Mediterranean Sea	May–Jun 1996	67	Uitz et al. [2006] and Peloquin et al. [2013]
Olipac	OL	Equatorial Pacific	Nov 1994	44	Claustre et al. [1999], Uitz et al. [2006], and Peloquin et al. [2013]
Pomme1	P1	North Atlantic	Feb–Mar 2001	58	Claustre et al. [2005], Uitz et al. [2006], and Peloquin et al. [2013]
Pomme2	P2	North Atlantic	Mar–May 2001	65	Claustre et al. [2005], Uitz et al. [2006], and Peloquin et al. [2013]
Pomme3	P3	North Atlantic	Sep 2001	78	Claustre et al. [2005], Uitz et al. [2006], and Peloquin et al. [2013]
Prosope	PR	Mediterranean Sea	Sep 1999	63	Claustre et al. [2004], Uitz et al. [2006], and Peloquin et al. [2013]
Strasse	ST	Sub-tropical North Atlantic	Aug–Sep 2012	36	PI: Claustre and Ras
Tara	TA	Global Ocean	2009–2012	82	PI: Bricaud, Boss and Ras
Total				896	

measuring the concentration of a suite of accessory pigments that can be used to estimate the composition of phytoplankton communities. Here we utilized the diagnostic pigment-based approach of *Uitz et al.* [2006], based on *Claustre* [1994] and *Vidussi et al.* [2001], to estimate the biomass associated with three pigment-derived size classes, i.e., microphytoplankton, nanophytoplankton, and picophytoplankton. Seven major pigments are selected as being representative of distinct phytoplankton groups: fucoxanthin, peridinin, 19′-hexanoyloxyfucoxanthin, 19′-butanoyloxyfucoxanthin, alloxanthin, chlorophyll *b* + divinyl chlorophyll *b*, and zeaxanthin (abbreviations in Table 1).

The fractions of chlorophyll *a* concentration associated with each of the three phytoplankton classes (f_{micro}, f_{nano}, and f_{pico}) are derived from the following equations [*Uitz et al.*, 2006]:

$$f_{micro} = \frac{(1.41\ [\text{Fuco}] + 1.41\ [\text{Perid}])}{\sum DP} \tag{1}$$

$$f_{nano} = \frac{(1.27\ [\text{Hex-fuco}] + 0.35\ [\text{But-fuco}] + 0.60[\text{Allo}])}{\sum DP} \tag{2}$$

$$f_{pico} = \frac{(1.01 \ [TChlb] + 0.86 \ [Zea])}{\sum DP} \tag{3}$$

with $\sum DP$ representing the sum of the seven diagnostic pigments concentrations:

$$\sum DP = 1.41 \ [Fuco] + 1.41 [Perid] + 1.27 [Hex - fuco] + 0.35 [But - fuco] + 0.60 [Allo] + 1.01 [TChlb] + 0.86 [Zea] \tag{4}$$

It is then possible to derive the chlorophyll *a* concentration associated with each of the three phytoplankton classes ([microChl], [nanoChl], and [picoChl]) according to the following equations:

$$[microChl] = f_{micro} * [TChl] \tag{5}$$

$$[nanoChl] = f_{nano} * [TChl] \tag{6}$$

$$[picoChl] = f_{pico} * [TChl] \tag{7}$$

The pigment-based approach of *Uitz et al.* [2006], admittedly, has some limitations. For example, some diagnostic pigments are shared by several phytoplankton groups and some groups may cover a broad size range. Nevertheless, it has proven valuable at regional and global scales for apprehending the composition of phytoplankton assemblages, both in terms of taxonomic composition and size structure. Recently, some modifications to the *Uitz et al.* [2006] approach have been proposed [*Brewin et al.*, 2010; *Devred et al.*, 2011]. Yet, in a comparative study, *Brewin et al.* [2014] show that these modifications do not bring major changes to the pigment-derived size structure of phytoplankton communities. Hence, in the present study, we calculate the [microChl], [nanoChl], and [picoChl] following *Uitz et al.* [2006].

Finally, a quality control was applied to each HPLC-determined vertical pigment profile as described in *Uitz et al.* [2006], i.e., (1) samples with [TChl] lower than 0.001 mg m^{-3} were rejected, (2) the first sample has to be located between the surface and 10 m depth, (3) the last sample has to be taken at a depth greater or equal to the euphotic depth, Ze, defined as the depth at which the irradiance is reduced to 1% of its surface value, and (4) a minimum of four samples per profile is required. For this quality control procedure, Ze is estimated according to the method of *Morel and Berthon* [1989], by using the [TChl] profile derived from HPLC estimates.

The data set used in this study includes concurrent fluorescence vertical profiles and HPLC-determined [TChl], [microChl], [nanoChl], and [picoChl] at discrete depths. This data set is representative of a large variety of hydrological, biogeochemical and associated trophic conditions observed in the open ocean (Figure 2). First, the HPLC-fluorescence database is characteristic of a broad variety of hydrological conditions. For example, it includes measurements acquired in the North Atlantic during winter when the mixed layer depth may reach 700 m (CATCH cruise) as well as measurements from the Subtropical South Pacific Gyre when the average mixed layer depth in spring is $\sim$30 m (BIOSOPE cruise). Second, the database is representative of most trophic conditions (from oligotrophic to eutrophic waters) observed in the global ocean. The parameter $[TChl]_{Z_0}$ defined as the [TChl] integrated between the surface and the depth Z_0 describes these different trophic conditions. Z_0 is set as the depth at which the fluorescence profile returns to a constant background value (see Figures 3a and 3b and section 2.2 for the calculation details). Indeed, the data set appears to be representative of the global ocean as $[TChl]_{Z_0}$ covers 2 order of magnitude. The most oligotrophic conditions were found during the Malina cruise in the Arctic Ocean with a value of about 10 mg m^{-2}; similarly, the $[TChl]_{Z_0}$ minimum value measured during the BIOSOPE cruise is 18 mg m^{-2}. The most eutrophic conditions are also represented with some profiles acquired in the Labrador Sea during the spring bloom with $[TChl]_{Z_0}$ values of about 900 mg m^{-2}. Because our data set is representative of a broad variety of conditions, we expect that the method developed here will be applicable at a global scale in the open ocean.

The data set presented here was split into two subsets. One subset was used for training the MLP; the second data set was used for validating the MLP. These two independent data sets, respectively, including about 80% (717 profiles) and 20% (179 profiles) of the initial data set, were randomly built up from a random selection of stations. As both data sets should be representative of the open
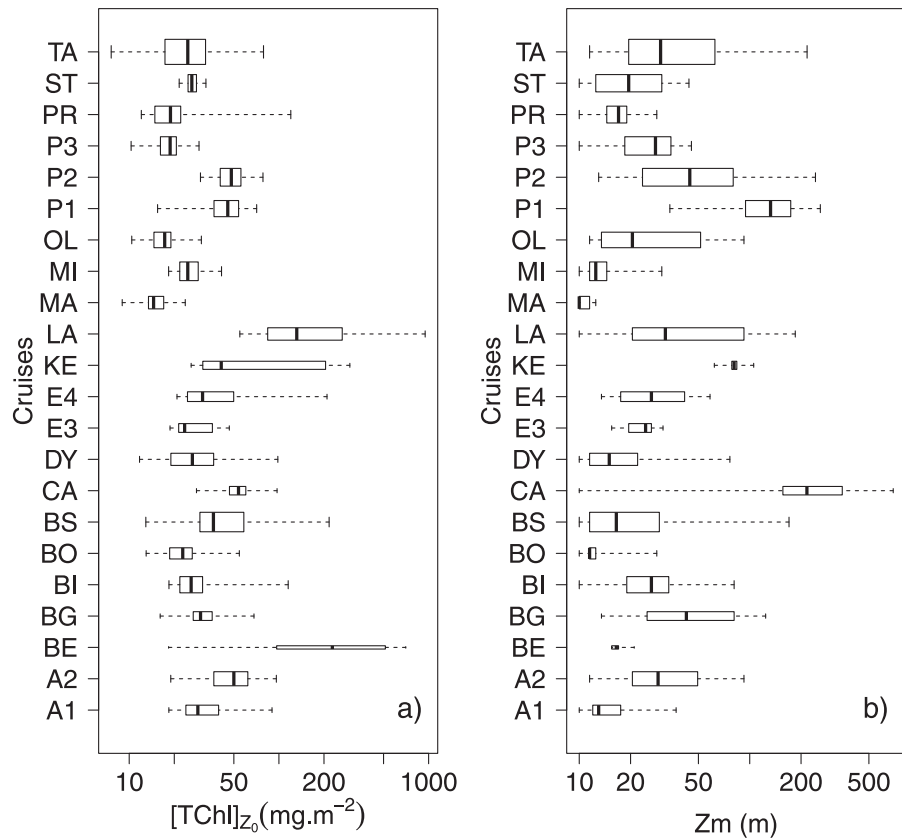
Figure 2. General characteristics of the data set used in this study. Boxplots of (a) the integrated [TChl] from the surface up to the depth Z_0, $[TChl]_{Z0}$ (mg m^{-2}), and (b) the mixed layer depth Z_m (m) for the 22 cruises. Boxplot widths vary depending on the cruise's number of data. The lower and upper whiskers represent the minimum to maximum values; the box represents the upper quartile and the lower quartile with the middle line representing the median of the values.

ocean, the stations were randomly selected from different trophic categories (Table 3), based on the concentration of chlorophyll *a* in the surface layer of the ocean, according to *Uitz et al.* [2006]. The geographic distribution of the sampling stations in the training and validation data sets is shown in Figures S1 and S2, respectively.

2.2. Data Processing

The FLAVOR algorithm has been developed on the basis of two dimensionless quantities. First, it is based on the shape of the fluorescence profile. Hence, all the fluorescence values of the database are normalized within the 0–1 range as follows:

$$fluo_{norm} = \frac{fluo - min(fluo)}{max(fluo) - min(fluo)} \quad (8)$$

with $fluo_{norm}$ the normalized fluorescence values and fluo the fluorescence in relative units. This procedure also enables merging fluorescence profiles from different sources and thus calibrated with different protocols or even uncalibrated.

Second, a dimensionless depth, ζ, is introduced and calculated as the actual depth, z, divided by Z_0:

$$\zeta = z/Z_0 \quad (9)$$

with Z_0 the depth at which the fluorescence profile returns to a constant background value. In order to compute Z_0, the $fluo_{norm}$ profile is smoothed using a median filter and the Z_0 depth is calculated as the first depth with a normalized fluorescence value of 0. As shown in Figure 3, the parameter Z_0 displays a large variability among the different fluorescence profiles of our database (17–831 m).
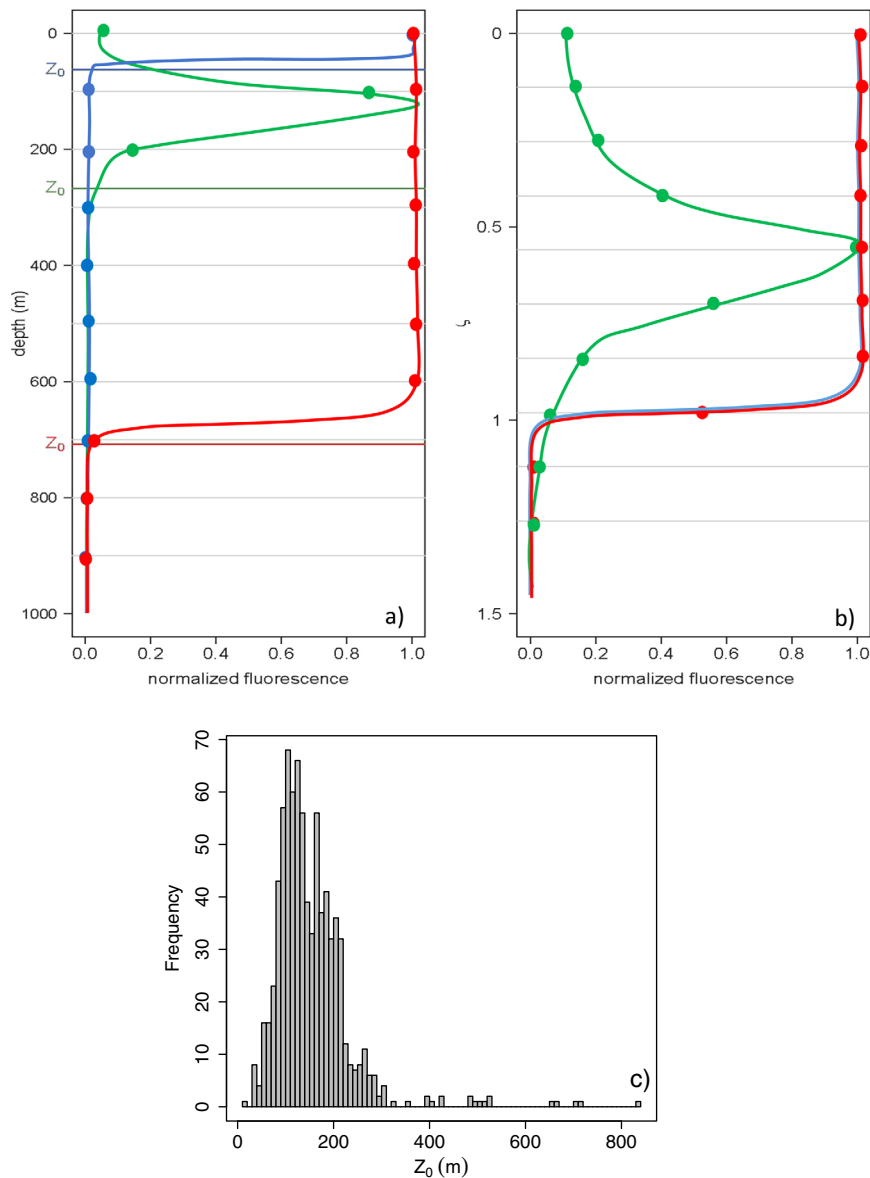
Figure 3. Characteristics of the fluorescence profile shape. (a) Three schematic normalized fluorescence profiles representative of the diversity of the observed situations; red: deeply mixed profile; green: stratified profile; blue: shallow mixed profile. Note that the corresponding Z_0 depths are reported. The lines correspond to the fluorescence profiles while the dots identify the hypothetical inputs of the fluorescence profiles for the MLP (10 inputs). (b) Same as for Figure 3a expect that the geometrical depth is here replaced by the dimensionless depth ζ. (c) Histogram of the Z_0 frequency distribution for the 896 fluorescence profiles of the database.

Scaling the fluorescence profiles with respect to ζ enables to merge all profiles regardless of their vertical shape and range of variation, simultaneously accounting for their variability. This normalization is an essential step because the MLP can only use as input discrete fluorescence values taken at fixed depths. Figure 3 shows three schematic examples of fluorescence profile, either non-normalized (Figure 3a) or depth-normalized (Figure 3b), obtained from contrasted open ocean environments, i.e., a typical profile of deep winter-mixing conditions (red curve), a profile with a Deep Chlorophyll Maximum (DCM) characteristic of stratified oligotrophic systems (green curve), and a profile with a subsurface maximum that can be encountered in mesotrophic or eutrophic environments with a relatively shallow mixed layer (blue curve). Based on the examination of Figure 3, it appears that, if the profile is not scaled with respect to depth, the 10 fixed-depth data

Table 3. Trophic Categories Defined According to *Uitz et al.* [2006] and Number of Sampling Stations in Each Category

Surface [TChl] (mg m^{-3})	Number of Stations
<0.04	102
0.04–0.08	206
0.08–0.12	116
0.12–0.2	117
0.2–0.3	81
0.3–0.4	46
0.4–0.8	128
0.8–2.2	70
2.2–4	18
>4	12

points used as input to the MLP may not account for all the vertical variability of the fluorescence profile.

3. FLAVOR Algorithm Development

In the following, [Chl] refers either to the chlorophyll *a* concentration associated with the total phytoplankton biomass ([TChl]) or with the microphytoplankton, nanophytoplankton, and picophytoplankton ([microChl], [nanoChl], and [picoChl], respectively).

Our proposed FLAVOR algorithm is based on an Artificial Neural Network (ANN). It uses as input data a normalized in situ vertical fluorescence profile along with the corresponding geo-location and date to retrieve vertical profiles of chlorophyll *a* associated with the total phytoplankton biomass ([TChl]) and with three phytoplankton size classes ([microChl], [nanoChl], and [picoChl]). FLAVOR is a two-step calibration method, as shown on the flowchart in Figure 4. First, a discrete (10-point) profile of [Chl] ([Chl]$_{MLP}$) is derived from an in situ fluorescence profile based on an ANN. The second step of the method consists in returning a quasi-continuous profile of [Chl] (i.e., with a vertical resolution identical as that of the in situ fluorescence profile, [Chl]$_{cal}$) based on the discrete ANN-derived [Chl] profile. This second step differs depending on the product to be returned by the ANN ([TChl] or [microChl], [nanoChl] and [picoChl]). Two different ANN-based algorithms are developed for inferring vertical profiles of either (1) [TChl] or (2) simultaneously [microChl], [nanoChl], and [picoChl].

3.1. Principles of Multilayer Perceptron (MLP)

The ANN used in this study is a Multilayered Perceptron (MLP) [*Bishop*, 1995] composed of four layers: one input layer, two hidden layers, and one output layer. In each layer, the neurons, which are elementary transfer functions, are interconnected with the neurons of the preceding and following layers by weights. The transfer of information through the MLP is done between the inputs I and outputs o and can be described as:

$$o = f(w^{2,o} \ f(w^{1,2} \ f(w^{i,1} \ I))) \qquad (10)$$

with f a sigmoid nonlinear function:

$$f(x) = a * \frac{\exp(\alpha.x) - 1}{\exp(\alpha.x) + 1} \qquad (11)$$

where a and α are two constants. In equation (10), $w^{i,1}$, $w^{1,2}$, and $w^{2,o}$ are the weight matrices that describe the connections between the input and first hidden layers, the first and second hidden layers, and the second hidden layer and the output layer, respectively. The coefficients of the weight matrix are iteratively readjusted during the training of the MLP in order to minimize a cost function defined as the quadratic difference between the desired and computed outputs. To this end, we used the back-propagation conjugate-gradient technique [*Hornik et al.*, 1989; *Bishop*, 1995], which is an iterative optimization method particularly adapted to MLPs. The training data set (80% of the entire initial data set) is further randomly split into two subdata sets (50% each), the so-called "learning" and "test" data sets. During the training process, these two subsets of data are used to cross validate the MLP and prevent from overlearning [*Bishop*, 1995]. Eventually, the validation data set used to evaluate the performance of the MLP is composed of 20% of the entire initial database.

3.2. Application of the MLP to the Chlorophyll Fluorescence and HPLC Pigment Database

Multiple tests were carried out to identify the optimal combination of input and output parameters which yield the best MLP performance. We selected the final following set of parameters as inputs (see also Figure 4): (1) 10 data points from the normalized fluorescence profile taken at regular intervals between the dimensionless depths 0 and 1.3; (2) the depth Z$_0$; (3) the dimensionless depth ζ at which [Chl] is to be computed; and (4) the location (latitude and longitude) and acquisition date (day of the year) of the considered fluorescence profile. Several tests were also performed to determine the optimal architecture of the MLP. Two types of architecture were tested: one or two hidden layers with a number of neurons in each layer varying between 1 and 50 and between 1 and
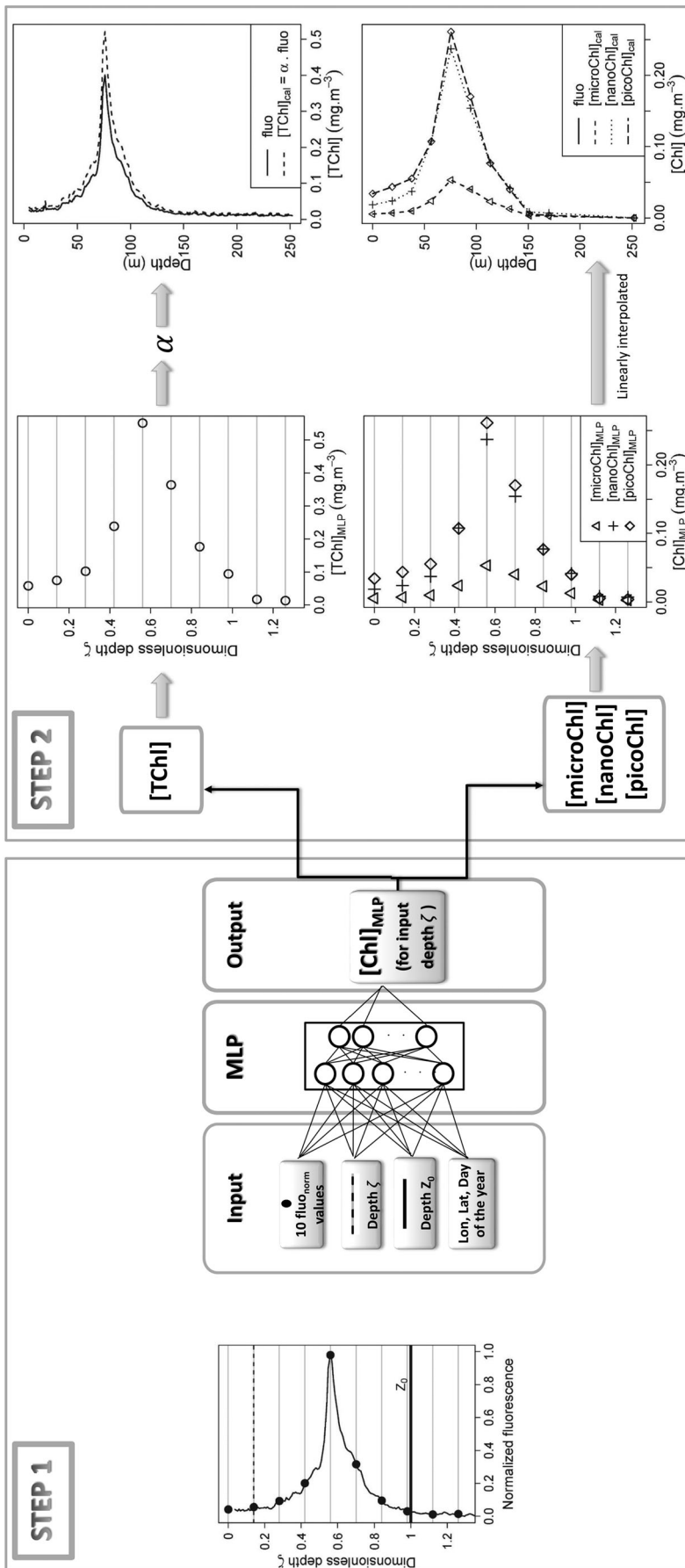
Figure 4. Schematic overview of the two steps involved in the FLAVOR method to retrieve a calibrated [Chl] profile from an uncalibrated fluorescence profile. Step 1: retrieval of a discrete [Chl] profile from the fluorescence profile through the use of a MLP. Step 2: retrieval of a continuous [Chl] profile from the discrete [Chl] profile retrieved by the MLP.

20, respectively (with the number of neurons always higher in the first hidden layer than in the second one in the case of two hidden layers). The optimal architecture was chosen as a compromise between a minimum error of validation and minimum number of neurons on the hidden layers to enhance computing efficiency.

Finally, the optimal architecture was a MLP composed of two hidden layers with seven neurons in the first hidden layer and seven neurons in the second one for the prediction of [TChl], and two hidden layers with nine neurons in the first hidden layer and five neurons in the second one for the simultaneous prediction of [microChl], [nanoChl], and [picoChl].

In addition, different partitions of the training data set have been tested for the validation of the MLP robustness. There were no significant differences in the performances of the MLP.

In order to take advantage of the nonlinearity of the function f (cf. equation (11)) that varies within the range $[-1;1]$, the inputs and outputs of the MLP are transformed to match the $[-1;1]$ domain, with respect to the following equation:

$$x_{i,j} = \frac{2}{3} * \frac{x_{i,j} - mean(x_{i,j})}{\sigma(x_{i,j})} \qquad (12)$$

with σ, the standard deviation of the considered input variables x or output variable log([Chl]).

For the longitude and date inputs, we applied a different normalization procedure that accounts for the periodicity of these properties. For example, the month of January (numerically identified as days 1 to 31) and the month of December (identified as days 334 to 365) are relatively similar from a seasonal perspective. In an analogous manner the longitude 0° is equivalent to the longitude 360°. Thus, these variables were transformed in radian units as follows:

$$Lon_{rad} = \frac{Lon * \pi}{180} \qquad (13)$$

$$Day_{rad} = \frac{Day * \pi}{182.625} \qquad (14)$$

where Lon_{rad} and Day_{rad} are the longitude and day of the year in radian units, respectively, and

the coefficient 182.625 accounts for the number of days per year (365.25) reduced by half.

As final inputs, we used the new variables $\sin(Lon_{rad})$, $\cos(Lon_{rad})$, $\sin(Day_{rad})$, and $\cos(Day_{rad})$ that vary within the interval $[-1;1]$. For example, $\cos(Day_{rad})$ is maximum in winter $(\cos(0) = 1)$ and minimum in summer $(\cos(\pi) = -1)$. Similarly, $\sin(Day_{rad})$ is maximum in spring $(\sin(\pi/2) = 1)$ and minimum in autumn $(\sin(3\pi/2) = -1)$. We note that, unlike the longitude and date, the latitude has no periodicity. Therefore, this variable was processed as the x inputs (cf. equation (12)).

3.3. Final Retrieval of Vertical Profiles of Chlorophyll *a* Concentration

The MLP returns 10 discrete normalized values of log([Chl]) as output. In the operational use of the MLP, the output needs to be "denormalized" (i.e., rescaled to physical units) using the inverse formulation of equation (12) with appropriate mean and standard deviation. The resulting discrete profiles of chlorophyll *a* concentration ($[Chl]_{MLP}$) are then transformed into calibrated vertical profiles ($[Chl]_{cal}$) with a resolution similar to that of the initial fluorescence profile used as input to the MLP. This procedure is different for the retrieval of [TChl] than for that of [microChl], [nanoChl], and [picoChl].

For the retrieval of the [TChl] vertical profile, we assumed that the in situ fluorescence profile yields the "true" shape of the [TChl] profile. The fluorescence profile used as input to the MLP is scaled to the chlorophyll *a* concentration using the discrete [TChl] values derived from the MLP ($[TChl]_{MLP}$). In other words, we forced the vertical fluorescence profile to the $[TChl]_{MLP}$ data points as in *Morel and Maritorena* [2001]. The new profile is then integrated within the layer $0–Z_0$ and used to compute the coefficient α:

$$\alpha = \frac{\int_0^{Z_0} [TChl]_{MLP}(z).dz}{\int_0^{Z_0} fluo(z).dz} \tag{15}$$

In order to obtain a final, calibrated high-vertical resolution [TChl] profile, each data point of the in situ fluorescence profile, fluo(z), is multiplied by the calibration coefficient α as follows:

$$[TChl]_{cal}(z) = \alpha \; . \; fluo(z) \tag{16}$$

The assumption that the fluorescence profile yields the actual vertical distribution of phytoplankton chlorophyll biomass is not applicable at the level of the phytoplankton size group because each group may have its own vertical distribution. Thus, the quasi-continuous final calibrated profiles of chlorophyll *a* concentration associated to the three size classes ($[microChl]_{cal}$, $[nanoChl]_{cal}$, and $[picoChl]_{cal}$) are derived directly from linear interpolation between the 10 discrete concentrations computed by the MLP for each size class.

3.4. Evaluation of the Method Performance

For the retrieval of [TChl] and the simultaneous retrieval of [microChl], [nanoChl], and [picoChl], the validation was done using an independent database, comprising 20% of our entire database (cf. section 2.1). This validation subset is composed of 179 chlorophyll fluorescence profiles with concomitant HPLC chlorophyll *a* reference values collected from 22 oceanographic cruises (Figure S2). The values retrieved from the FLA-VOR method were evaluated against in situ HPLC measurements at two different steps: (1) after the first step of the method (performance of the MLP); (2) after the second step of the method (performance of the full calibration method). To assess the first step method performance, the [Chl] derived from the MLP, $[CHL]_{MLP}$, is compared to the HPLC linearly interpolated for the 10 input depths (see Figure 4). For the assessment of the second step method performance, the quasi-continuous [Chl] profile, $[Chl]_{cal}$, is compared to HPLC values for each corresponding depths.

To evaluate the performance of the method, several statistical indices were utilized. We calculated the determination coefficient (R^2) and the slope of the linear regression between the computed calibrated fluorescence values and the in situ reference HPLC values. In addition, the Median Absolute Percent Difference (MAPD) between the reference and predicted values was computed:
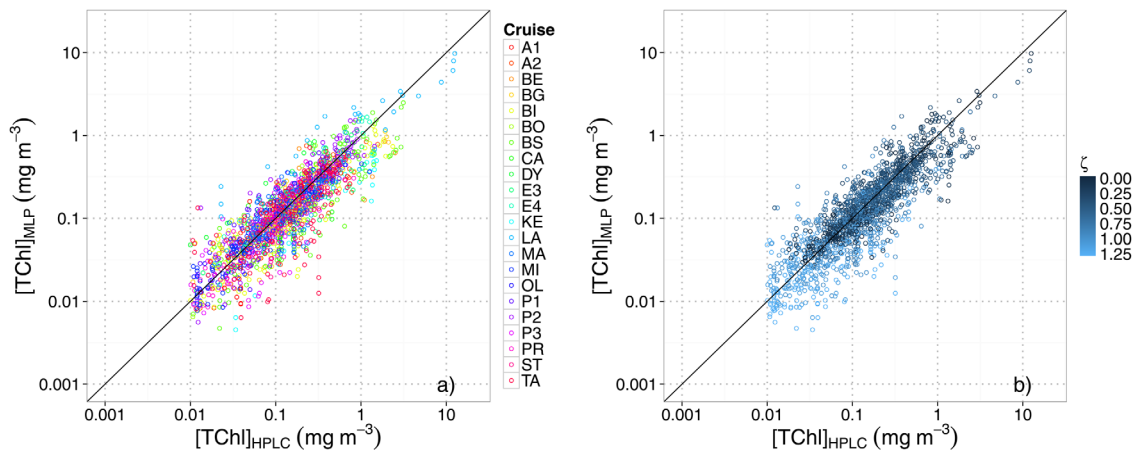
Figure 5. Comparison between [TChl] retrieved by the MLP ([TChl]$_{MLP}$) with HPLC reference ([TChl]$_{HPLC}$). (a) Data identified according to the 22 cruises and (b) data ordered according to the dimensionless depth ζ. The HPLC pigment reference values correspond to linear interpolation of the HPLC measurements for the 10 [TChl] restitution depths of the MLP. The 1:1 line is represented in black in each plot.

$$MAPD = \frac{(|fluo_{cal} - [Chl]|)}{[Chl]} * 100 \qquad (17)$$

As shown by *Campbell* [1995] the chlorophyll *a* concentration follows a lognormal distribution in the open ocean. Therefore, the values were log-transformed prior to the calculation of the statistical indices, except for the MAPD.

4. Results and Discussion

4.1. Retrieval of Chlorophyll *a* Concentration Associated With the Total Phytoplankton Biomass

The accurate retrieval of [TChl] relies both on the performance of the MLP (first step of the method) and on the subsequent application of the calibration coefficient α (second step; cf. Figure 4). The scatterplot of the [TChl] values retrieved from the MLP versus those measured by HPLC (Figure 5) reveals that the data are fairly well distributed around the 1:1 line (see also Table 4 for detailed statistics). This relationship does not show any bias related to the sampling cruise (Figure 5a), therefore suggesting that the proposed method is relatively robust both spatially and temporally. To verify this statement, the relationships between the [TChl] values retrieved from the MLP and measured by HPLC were computed for eight major oceanic basins: Antarctic, Arctic, Mediterranean Sea, Indian, South Pacific, North Pacific, South Atlantic, and North Atlantic Ocean (Figure S3). The determination coefficient, R^2, and the MAPD between the retrieved and reference values for the different basins indicate that the method is robust, with slightly less accurate results for the Arctic basin and the Indian Ocean which are two areas known for data scarcity (see Figure S4). Nevertheless, Figure 5b shows more scatter at low chlorophyll levels which, in general, correspond to the greatest dimensionless depths ζ. This observation supports the results shown in Figure 6 where the determination coefficients and the MAPD between the [TChl] values derived from the MLP and measured by HPLC were computed for six dimensionless depth intervals. The determination coefficient R^2 decreases with increasing ζ, whereas the corresponding MAPD increases with increasing ζ. This supports the idea that the MLP is less robust for retrieving [TChl] values at large depths. Nevertheless, the relationship between [TChl]$_{MLP}$ and [TChl]$_{HPLC}$ for each of the six dimensionless depth intervals is significant ($p_{value} < 0.005$). Furthermore, it should be noticed that the retrieval of [TChl]$_{MLP}$ is
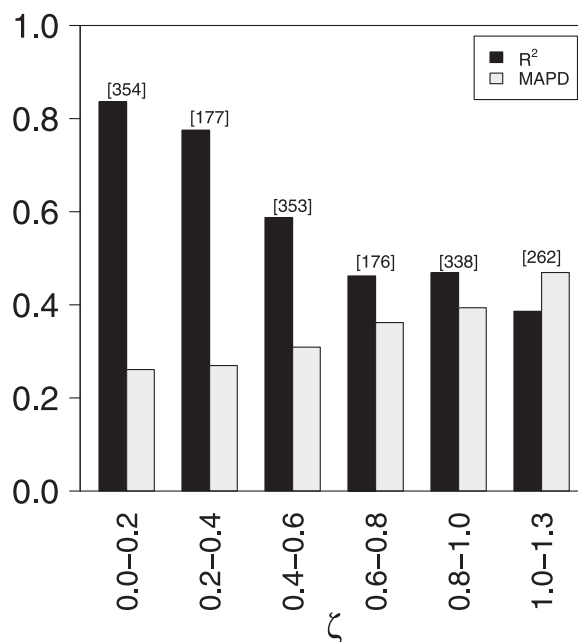
Table 4. Comparison of Values Retrieved by the MLP ([Chl]$_{MLP}$, First Step of Calibration) or Through the Second Step of Calibration ([Chl]$_{cal}$) With Concomitant HPLC Reference Values ([Chl]$_{HPLC}$)[a]

	R^2	a	MAPD (%)
First Step			
[TChl]$_{MLP}$	0.74	0.83	32
[microChl]$_{MLP}$	0.73	0.78	44
[nanoChl]$_{MLP}$	0.60	0.69	35
[picoChl]$_{MLP}$	0.57	0.64	44
Second Step			
[TChl]$_{cal}$	0.68	0.96	40
[microChl]$_{cal}$	0.72	0.75	46
[nanoChl]$_{cal}$	0.64	0.68	35
[picoChl]$_{cal}$	0.58	0.61	40

[a]Determination coefficient (R^2) and slope (a) corresponding to linear regression analyses between retrieved and reference values. For each case, the MAPD (Median Absolute Percent Difference) between retrieved and reference values is also indicated.

Figure 6. Determination coefficient R^2 and Median Absolute Percent Difference (MAPD) of the linear models between [TChl] retrieved by the MLP ([TChl]$_{MLP}$) and HPLC reference ([TChl]$_{HPLC}$) values computed for several dimensionless depth intervals. The number of points corresponding to each interval is identified in bracket. The MAPD is presented here divided by 100 so values range is 0–1.

less critical for deeper layers than for upper layers where most of the phytoplankton biomass occurs. The calibration coefficient α applied to the in situ fluorescence profile takes into account only the MLP-predicted values comprised between surface and Z_0 (cf. section 3.3).

The second step of our method allows the retrieval of calibrated [TChl] ([TChl]$_{cal}$) profiles with the same vertical resolution as the initial fluorescence profiles. The performance of the method is assessed through the comparison of [TChl]$_{cal}$ with the corresponding in situ HPLC measurements, [TChl]$_{HPLC}$ (Figure 7 and Table 4). The relationship between [TChl]$_{cal}$ and [TChl]$_{HPLC}$ appears more scattered than the relationship between [TChl]$_{MLP}$ and [TChl]$_{HPLC}$ (i.e., first step of the method; Figure 5 and Table 4). This might be due, at least partially, to the reintroduction of the signal noise of the in situ measured fluorescence profile into the MLP-retrieved profile that can be sometimes particularly pronounced. However, compared with the HPLC reference values, the fluorescence profiles calibrated into [TChl] appear globally unbiased.

The impact of the daytime Non-Photochemical Quenching (NPQ) [see, e.g., *Cullen and Lewis*, 1995], which is responsible for a reduction in the chlorophyll fluorescence at high irradiance, deserves further consideration in the evaluation of the proposed method. In the first step of FLAVOR, the MLP learning is based on in situ measurements so that the NPQ is implicitly taken into consideration and thus corrected for a proper restitution of the chlorophyll *a* concentration (i.e., to a given quenched chlorophyll fluorescence profile is associated an unquenched HPLC-determined chlorophyll *a* profile). In the second step of FLAVOR, the initial fluorescence profile shape is used to compute the final [TChl]$_{cal}$ (see equation (16)); thus, the potential bias due to the NPQ is implicitly reintroduced. This is admittedly a weakness of the present method. If density profiles are acquired simultaneously to fluorescence profiles, the NPQ could be corrected following the method of *Xing et al.* [2012]. This method involves substituting the fluorescence values acquired within the mixed layer by the maximum value within this layer. If the concomitant acquisition of density is not available, there is presently no solution to overcome the potential issue of the NPQ.

Finally, the performance of FLAVOR can be compared with that of other methods developed to retrieve the vertical distribution of the total chlorophyll *a* concentration from fluorescence profiles. The method proposed by *Lavigne et al.* [2012] was evaluated using the long-term time series data sets from the BATS, HOT, and Dyfamed stations. The method developed by *Mignot et al.* [2011] and the method presented here were evaluated with data sets representative of the global ocean. Although the performances of these three methods were assessed on the basis of different data sets, the statistical indices of performance of these methods can be compared, at least in an indicative manner. The MAPD is 33%, 31% and 32% for the methods developed by *Mignot et al.* [2011], *Lavigne et al.* [2012] and FLAVOR, respectively. In other words, FLAVOR performs well in comparison to the other methods and presents the additional advantage of being self-sufficient, i.e., it does not require any other external information or data to retrieve the phytoplankton total or class-specific chlorophyll *a* concentration (except the geo-location and date of acquisition which
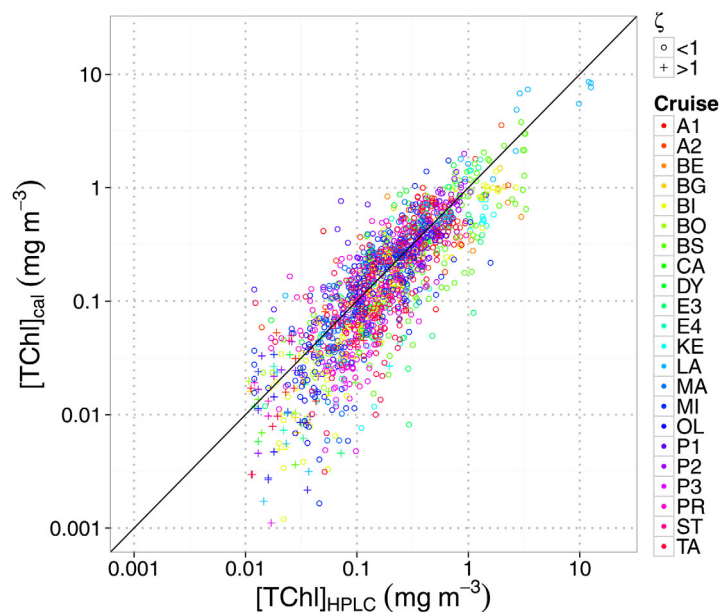
Figure 7. Comparison between [TChl] retrieved by the calibration method ([TChl]$_{cal}$) and reference HPLC values ([TChl]$_{HPLC}$) for the 22 cruises analyzed in this study. The cruises are represented by different colors and according to two intervals of dimensionless depths ($\zeta < 1$: circle; and $\zeta > 1$: cross). The 1:1 line is represented in black.

are information always available with the fluorescence profiles). For instance, the method of *Lavigne et al.* [2012] uses the remotely sensed surface chlorophyll *a* concentration as additional input information, whereas that of *Mignot et al.* [2011] requires a classification of fluorescence profiles into two types of shapes (mixed or stratified).

4.2. Retrieval of Chlorophyll *a* Concentration Associated With the Three Phytoplankton Size Classes

The performance of FLAVOR is here evaluated for the retrieval of chlorophyll *a* profiles associated with the three phytoplankton pigment-based size classes from in situ fluorescence profiles. For the first step
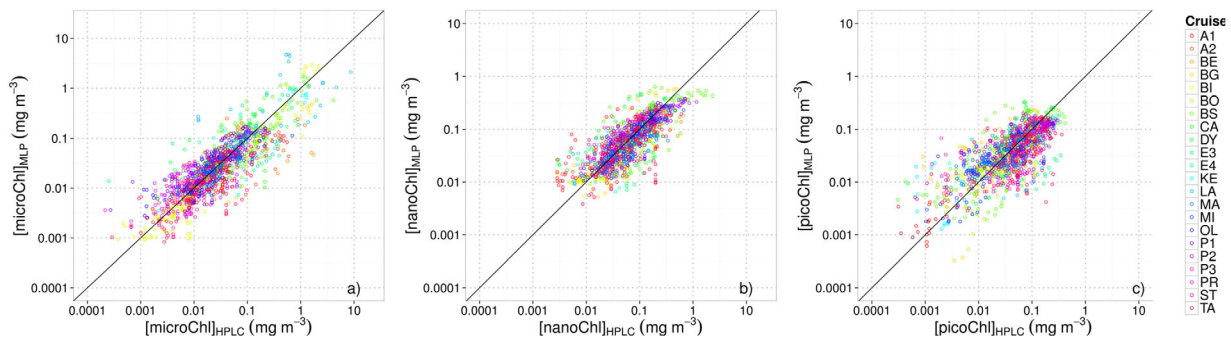
of the method, there is a reasonably good agreement between the MLP-retrieved values (i.e., [microChl]$_{MLP}$, [nanoChl]$_{MLP}$, and [picoChl]$_{MLP}$) and the corresponding in situ HPLC determinations (Figure 8 and Table 4); no systematic bias is observed. The method performance is higher for [microChl] that presents the largest range of variation of the three size classes (0.0003–10 mg m^{-3}), than for [picoChl] that varies over a limited range of relatively low concentrations (0.0005–0.3 mg m^{-3}). The method performance is intermediate for [nanoChl] that varies over a limited range of moderate concentrations (0.003–3 mg m^{-3}). In addition, the relationships between the MLP-retrieved and reference in situ values were computed for eight major oceanic basins (see Figure S3 and section 4.1). Figures S5–S7, which display the determination coefficients R^2 and the MAPD between the retrieved and reference values for the different basins, show that the method is relatively robust spatially.

The performance of the calibration method is now evaluated after the second step of the method (see Figure 4) which allows the retrieval of "high-resolution" vertical profiles of [microChl]$_{cal}$, [nanoChl]$_{cal}$, and [picoChl]$_{cal}$. The relationships between these derived quantities and their HPLC-determined counterparts (Figure 9) are quite similar to those observed at the first step of the calibration method (cf. Figure 8). These results are coherent with the statistical analysis (Table 4) that confirms that the second step of the calibration method does not deteriorate the initial, MLP-based retrieval of [microChl]$_{MLP}$, [nanoChl]$_{MLP}$, and [picoChl]$_{MLP}$ (first step of the method). On Figure 9, a few outliers can be identified, which are related to the very low chlorophyll *a* concentrations typical of very deep samples.

When studying the specific [Chl]$_{cal}$ profiles individually, their vertical distributions appear closely similar to the vertical distributions of their corresponding discrete profiles estimated by HPLC (data not shown). This observation is important for validating the present method because the second step of the calibration is here not "forced" as for the [TChl] retrieval. As might be expected, we verified that the retrieval of [TChl] is better with a specific MLP than through the sum of [microChl], [nanoChl], and [picoChl] retrieved simultaneously by the MLP. This likely results from the addition of errors associated with each of the three retrieved specific [Chl], whereas for the retrieval of the [TChl], only one error of prediction is involved. However, the retrieval of [TChl] is coherent with the sum of [microChl], [nanoChl], and [picoChl] retrievals as there is no systematic bias between both quantities when compared with a linear model (R^2 = 0.81 and slope = 0.97).

In summary, compared with the HPLC reference values, the fluorescence profiles calibrated simultaneously into [microChl], [nanoChl], and [picoChl] are globally unbiased, with R^2 values of 0.72, 0.64, and 0.58,

Figure 8. Comparison between [Chl] retrieved by the MLP ([Chl]$_{MLP}$) and measured by HPLC ([Chl]$_{HPLC}$) for the three pigment size classes [Chl]. (a) [microChl], (b)[nanoChl], and (c) [picoChl]. The HPLC pigment reference values correspond to a linear interpolation of the HPLC measurements for the 10 [Chl] restitution depths of the MLP. Each color refers to one of the 22 cruises analyzed in this study. The 1:1 line is represented in black in each plot.

respectively, and a median error of 46%, 35%, and 40%, respectively (Table 4). The slightly lower performances of the retrieval of the vertical distribution of [microChl], [nanoChl] and [picoChl] compared to that of [TChl] is essentially caused by a larger natural variability introduced by the different phytoplankton communities.

4.3. Possible Application: Development of Global and Regional 3-D Climatologies of Chlorophyll *a* Concentration and Associated Phytoplankton Communities

FLAVOR can be considered as a robust method to reconcile fluorescence profiles from extremely diverse sources (with respect to both sensors and platforms) by converting these profiles into a common "reference": the vertical profile of chlorophyll *a* concentration. To our knowledge, it is so far the only method that allows various fluorescence data sets to become interoperable. This potential interoperability not only concerns the "historical" data from diverse origins used in this study, but also the data that will be acquired in the future. This especially concerns the tremendous amount of fluorescence profiles that will likely result from the growing use of autonomous platforms such as bio-optical profiling floats [*Claustre et al.*, 2010b]. The FLAVOR algorithm is, obviously, less accurate than dedicated analytical methods (HPLC) for determining the chlorophyll *a* concentration associated with the total phytoplankton biomass or with three major size classes. Nevertheless, this lower accuracy is largely compensated by the potential of our method to process a larger amount of data, covering a much larger space and time domain. As supported by our statistical results, we argue that FLAVOR could be used to produce climatologies of chlorophyll *a* concentration profiles by using as input large amounts of historical and modern fluorescence data.

To illustrate such potential, the FLAVOR method was applied to the BATS (Bermuda Atlantic Time Series Study) site where a large amount of HPLC and fluorescence profiles have been acquired over the 1998–2012 time period. In this data set, there are approximately twenty times more fluorescence profiles available
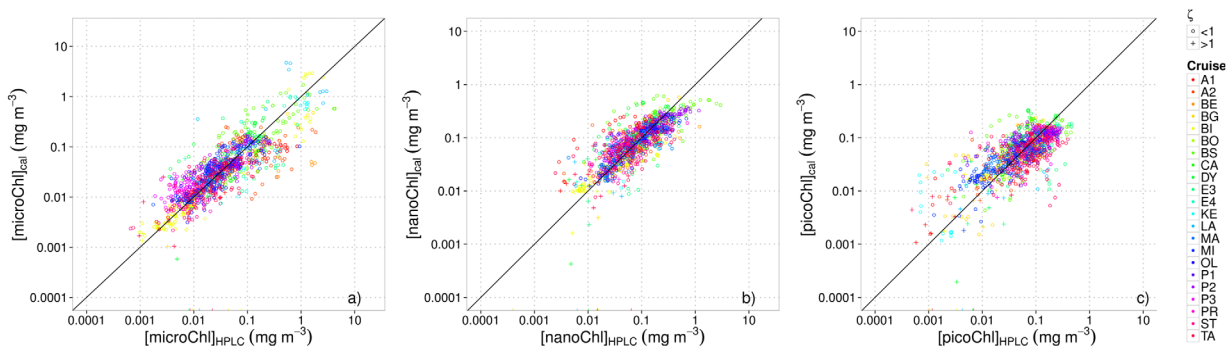

Figure 9. Comparison between [Chl] retrieved by the calibration method ([Chl]$_{cal}$) and measured by HPLC ([Chl]$_{HPLC}$) for the three pigment size classes (a) [microChl], (b) [nanoChl], and (c) [picoChl]. The 22 cruises analyzed in this study are represented by different colors and according to two intervals of dimensionless depths ($\zeta < 1$: circle; and $\zeta > 1$: cross). The 1:1 line is represented in black in each plot.
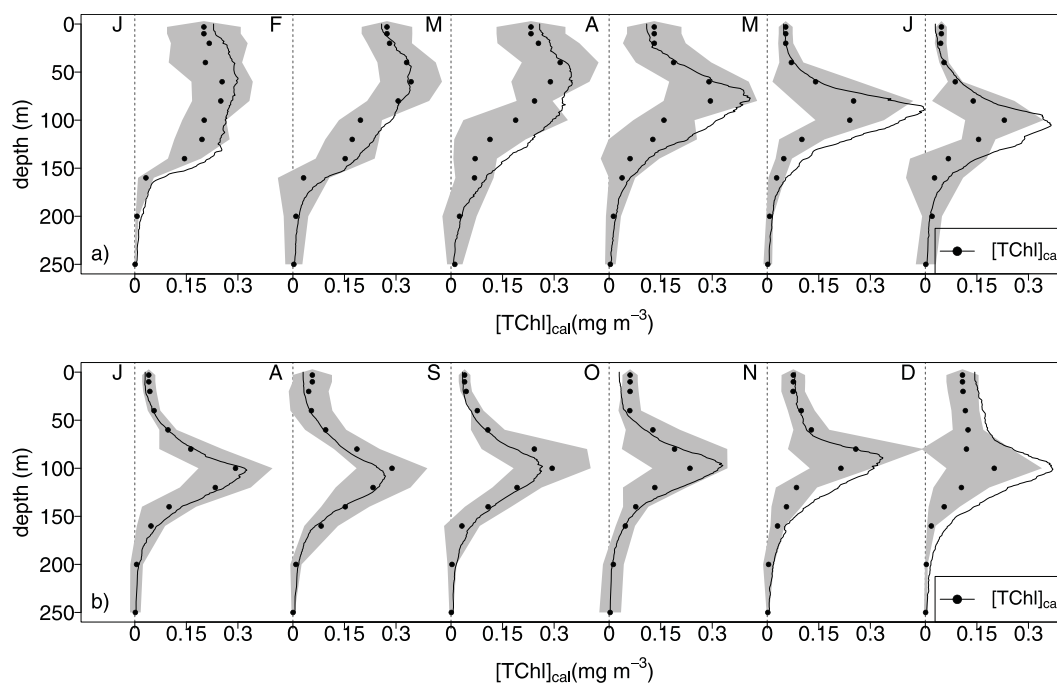
Figure 10. Bermuda Atlantic Time series Study: comparisons of the monthly climatologies of HPLC-based chlorophyll *a* concentrations ([TChla]$_{HPLC}$ in dots) with FLAVOR-retrieved chlorophyll *a* concentrations ([TChl]$_{cal}$ in continuous black line). The gray polygons represent the standard deviation of the HPLC-based climatology. (a) Comparisons presented for the months from January to June. (b) Comparisons presented for the months from July to December.

than HPLC discrete profiles. Hence, in addition to the benefit of providing depth-continuous chlorophyll *a* profiles, our method enables to process all fluorescence profiles thus providing twenty times more profiles than the HPLC method in this region. It is worth to note that this data set was not taken into account for the training of our method. Figure 10 shows monthly climatological fluorescence profiles calibrated into [TChl] compared with the corresponding HPLC measurements. Overall, the monthly pattern in the climatological [TChl]$_{HPLC}$ profiles is well reproduced by the fluorescence-based climatological profiles retrieved from the algorithm. The fluorescence-based climatological profiles indeed generally fall within one standard deviation of the HPLC-based climatological profiles. The observed deviations (i.e., climatological fluorescence profiles outside the envelope of one standard deviation of [TChl]$_{HPLC}$ in Figure 10) can obviously be linked to a FLAVOR failure and/or to the use of climatologies. Nevertheless, the observed deviations might also result from the availability of more fluorescence than HPLC profiles in the BATS database. As a result, the fluorescence records might have captured a broader diversity of situations (e.g., some local events associated to mesoscale activity). Another explanation may be a bias in the HPLC-based climatology caused by sampling at fixed depths, which potentially misses certain vertical features such as a DCM. In any case, the overall agreement between both the fluorescence- and HPLC-based climatological chlorophyll *a* profiles remains satisfactory considering that no BATS data were present in the MLP learning database. This comparison also indicates that our method is not location biased. Thus, the present analysis clearly stands as an additional and independent validation, confirming the robustness of the FLAVOR method. It is also an a posteriori confirmation that the training data set is likely representative of the full range of situations occurring in open ocean waters.

Besides the retrieval of chlorophyll *a* concentration associated with the total phytoplankton biomass ([TChl]), the retrieval of the phytoplankton class-specific chlorophyll *a* concentration ([Chl]) was also evaluated (Figure 11). As expected, the performance of the method for retrieving [Chl] is not as good as for retrieving [TChl]. Nevertheless the fluorescence-based monthly climatologies of [Chl] associated with the three phytoplankton size classes compare relatively well with the corresponding HPLC-based climatologies. Again, given the independence of the BATS data set with respect to MLP training data set, these results appear very promising.
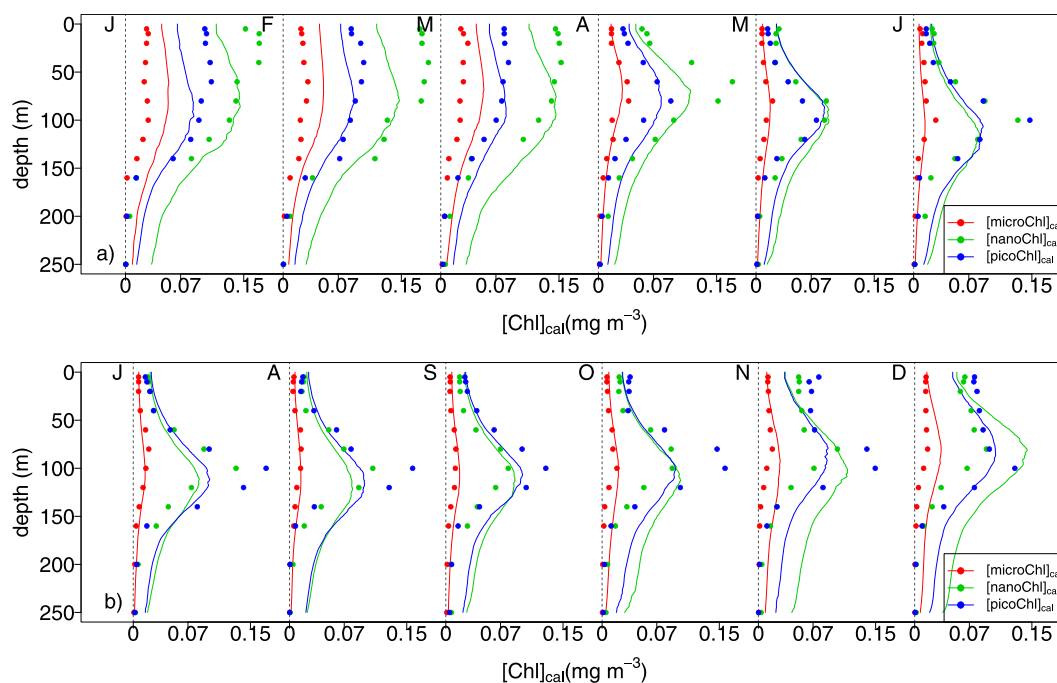
Figure 11. Bermuda Atlantic Time series Study: comparisons of the monthly climatologies of HPLC-based chlorophyll *a* concentrations associated to phytoplankton community size indices ([Chl]$_{HPLC}$ in dots) with FLAVOR-retrieved concentrations ([Chl]$_{CAL}$ in continuous lines). Red: [microChl]; green: [nanoChl]; blue: [picoChl]. (a) Comparisons presented for the months from January to June. (b) Comparisons presented for the months from July to December.

The above application of FLAVOR to the BATS time series can be considered as a preview of the future of climatological fields of the vertical distribution of phytoplankton chlorophyll *a* biomass and associated community composition at a global scale as well as for specific regions. To our knowledge, the current climatologies of chlorophyll *a* concentration available in the World Ocean Atlas (WOA) [*Conkright et al.*, 2002] are based on fixed depths (discrete data) and with no concurrent quantitative information on phytoplankton assemblages. The utilization of large data sets of fluorescence profiles will offer very significant improvements over existing climatologies. Quantitatively it will be possible to have access to an increasing amount of data with enhanced time and space resolution measurements. A parallel can be made with CTD-based temperature and salinity profiles for which, thanks to the development of the Argo program and the million profiles achieved in 2012, robust climatologies are now available.

Apart from a quantitative estimation of phytoplankton biomass through chlorophyll *a* concentration, the possibility of further separating this biomass into three main phytoplankton size groups is also of crucial importance. It is indeed recognized that taking into consideration the nature of the phytoplankton assemblage is key in addressing the marine carbon cycle in a more comprehensive way, for example, using bio-optical [*Uitz et al.*, 2010] or biogeochemical modeling [*Aumont et al.*, 2003; *Le Quere et al.*, 2005; *Hood et al.*, 2006]. FLAVOR will allow the provision of global-scale data required for the initialization and/or validation of such models. The quality and representativeness of the data sets used for the initialization and validation of modeling approaches will improve over time as the density of fluorescence data sets progressively increases.

5. Conclusions and Perspectives

The FLAVOR method allows the assessment of the vertical distribution of phytoplankton chlorophyll *a* biomass and associated phytoplankton communities from in situ chlorophyll fluorescence profile. Based on an Artificial Neural Network, FLAVOR enables the retrieval of the chlorophyll *a* concentration profiles associated (1) with the total phytoplankton biomass and (2), simultaneously, with three pigment-derived size classes, from the sole knowledge of the shape of the fluorescence profile and its acquisition date and geo-location. Consequently, for the first time, the large data set of fluorescence profiles collected

since the 1970s could be harmonized and made interoperable in terms of chlorophyll *a* concentration. Additionally, it is the first method that allows for the retrieval of the composition of phytoplankton communities from a fluorescence profile. However, it is important to note that to apply the method to fluorescence profiles acquired pre-1991, the assumption has to be made that the relationship between the phytoplankton biomass and the community composition with the fluorescence profile is the same as for our data set (post 1991).

Validation results have been presented here regarding the retrieval of total and class-specific chlorophyll *a* concentration versus in situ HPLC reference measurements. Our method appears to be spatially and temporally robust as the relationships between the retrieved and reference in situ values do not show systematic bias with respect to the different oceanic regions and cruises regardless of the product to be retrieved (Figures 5a and 7–9 and Figures S4–S7). Additionally, because FLAVOR was developed using a data set that is representative of most of the hydrologic and trophic conditions prevailing in the open ocean, it can be considered potentially applicable to any situation occurring in the global open ocean. Nevertheless, it should be emphasized that, although FLAVOR is applicable to situations in which it has not been trained (e.g., the BATS time series; see Figures 10 and 11), its use deserves some caution. FLAVOR is not a method for use on a profile-by-profile basis, where a single fluorescence profile would be injected to retrieve accurate profiles of chlorophyll *a* concentration for the entire algal biomass and associated size indices. Instead, the method is intended for use on large data sets for deriving vertical chlorophyll *a* climatologies from which some regional or temporal trends might possibly be extracted. Such data sets could be exploited to improve the open ocean climatologies of chlorophyll *a* concentration.

Hence, thanks to the ongoing and future availability of spatially and temporally well-resolved data sets, it will become possible to develop 3-D and even 4-D global climatologies of chlorophyll *a* concentration and associated community composition in terms of three major phytoplankton size classes. These types of climatologies are not only required for the initialization and validation of biogeochemical models but may also serve as benchmark for documenting possible changes in phytoplankton biomass and distribution in the global ocean.

References

Aumont, O., E. Maier-Reimer, S. Blain, and P. Monfray (2003), An ecosystem model of the global ocean including Fe, Si, P colimitations, *Global Biogeochem. Cycles*, *17*(2), 1060, doi:10.1029/2001GB001745.

Ben Mustapha, Z., S. Alvain, C. Jamet, H. Loisel, and D. Dessailly (2013), Automatic classification of water-leaving radiance anomalies from global SeaWiFS imagery: Application to the detection of phytoplankton groups in open ocean waters, *Remote Sens. Environ.*, *146*, 97–112, doi:10.1016/j.rse.2013.08.046.

Bishop, C. M. (1995), *Neural Networks for Pattern Recognition*, 482 pp., Oxford Univ. Press, Oxford, U. K.

Brewin, R. J. W., S. Sathyendranath, T. Hirata, S. J. Lavender, R. M. Barciela, and N. J. Hardman-Mountford (2010), A three-component model of phytoplankton size class for the Atlantic Ocean, *Ecol. Modell.*, *221*(11), 1472–1483, doi:10.1016/j.ecolmodel.2010.02.014.

Brewin, R. J. W., S. Sathyendranath, P. K. Lange, and G. Tilstone (2014), Comparison of two methods to derive the size-structure of natural populations of phytoplankton, *Deep Sea Res., Part I*, *85*, 72–79, doi:10.1016/j.dsr.2013.11.007.

Bricaud, A., E. Bosc, and D. Antoine (2002), Algal biomass and sea surface temperature in the Mediterranean Basin, *Remote Sens. Environ.*, *81*(2–3), 163–178, doi:10.1016/S0034-4257(01)00335-2.

Bricaud, A., C. Mejia, D. Blondeau-Patissier, H. Claustre, M. Crepon, and S. Thiria (2007), Retrieval of pigment concentrations and size structure of algal populations from their absorption spectra using multilayered perceptrons, *Appl. Opt.*, *46*(8), 1251–1260.

Buitenhuis, E. T., et al. (2012), Picophytoplankton biomass distribution in the global ocean, *Earth Syst. Sci. Data*, *4*(1), 37–46, doi:10.5194/essd-4-37-2012.

Campbell, J. W. (1995), The lognormal distribution as a model for bio-optical variability in the sea, *J. Geophys. Res.*, *100*(C7), 13,231–13,254.

Claustre, H. (1994), The trophic status of various oceanic provinces as revealed by phytoplankton pigment signatures, *Limnol. Oceanogr.*, *39*(5), 1206–1210.

Claustre, H., and J.-C. Marty (1995), Specific phytoplankton biomasses and their relation to primary production in the tropical North Atlantic, *Deep Sea Res., Part I*, *42*(8), 1475–1493, doi:10.1016/0967-0637(95)00053-9.

Claustre, H., P. Kerhervé, J. C. Marty, L. Prieur, C. Videau, and J.-H. Hecq (1994), Phytoplankton dynamics associated with a geostrophic front: Ecological and biogeochemical implications, *J. Mar. Res.*, *52*(4), 711–742, doi:10.1357/0022240943077000.

Claustre, H., A. Morel, M. Babin, C. Cailliau, D. Marie, J.-C. Marty, D. Tailliez, and D. Vaulot (1999), Variability in particle attenuation and chlorophyll fluorescence in the tropical Pacific: Scales, patterns, and biogeochemical implications, *J. Geophys. Res.*, *104*(C2), 3401–3422, doi:10.1029/98JC01334.

Claustre, H., F. Fell, K. Oubelkheir, L. Prieur, A. Sciandra, B. Gentili, and M. Babin (2000), Continuous monitoring of surface optical properties across a geostrophic front: Biogeochemical inferences, *Limnol. Oceanogr.*, *45*(2), 309–321.

Claustre, H., et al. (2004), An intercomparison of HPLC phytoplankton pigment methods using in situ samples: Application to remote sensing and database activities, *Mar. Chem.*, *85*(1–2), 41–61, doi:10.1016/j.marchem.2003.09.002.

Claustre, H., M. Babin, D. Merien, J. Ras, L. Prieur, S. Dallot, O. Prasil, H. Dousova, and T. Moutin (2005), Toward a taxon-specific parameterization of bio-optical models of primary production: A case study in the North Atlantic, *J. Geophys. Res.*, *110*, C07S12, doi:10.1029/2004JC002634.

Claustre, H., et al. (2010a), Bio-optical profiling floats as new observational tools for biogeochemical and ecosystem studies: Potential synergies with ocean color remote sensing, in *Proceedings of the OceanObs 09: Sustained Ocean Observations and Information for Society Conference*, vol. 2, edited by J. Hall, D. E. Harrison, and D. Stammer, ESA Publ., Venice, Italy.

Claustre, H., et al. (2010b), Guidelines towards an integrated ocean observation system for ecosystems and biogeochemical cycles, in *Proceedings of the OceanObs 09: Sustained Ocean Observations and Information for Society Conference*, vol. 1, edited by J. Hall, D. E. Harrison, and D. Stammer, ESA Publ., Venice, Italy.

Conkright, M. E., R. A. Locarnini, H. E. Garcia, T. D. O'Brien, T. P. Boyer, C. Stephens, and J. I. Antonov (2002), *World Ocean Atlas 2001: Objective Analyses, Data Statistics, and Figures* [CD-ROM], U.S. Dep. of Commer., Natl. Oceanic and Atmos. Admin., Natl. Oceanogr. Data Cent., Ocean Clim. Lab., Silver Spring, Md.

Crombet, Y., K. Leblanc, B. Quéguiner, T. Moutin, P. Rimmelin, J. Ras, H. Claustre, N. Leblond, L. Oriol, and M. Pujo-Pay (2011), Deep silicon maxima in the stratified oligotrophic Mediterranean Sea, *Biogeosciences*, *8*(2), 459–475, doi:10.5194/bg-8-459-2011.

Cullen, J. J., and M. R. Lewis (1995), Biological processes and optical measurements near the sea surface: Some issues relevant to remote sensing, *J. Geophys. Res.*, *100*(C7), 13,255–13,266, doi:10.1029/95JC00454.

Cunningham, A. (1996), Variability of in-vivo chlorophyll fluorescence and its implication for instrument development in bio-optical oceanography, *Sci. Mar.*, *60*(1), 309–315.

Devred, E., S. Sathyendranath, V. Stuart, and T. Platt (2011), A three component classification of phytoplankton absorption spectra: Application to ocean-color data, *Remote Sens. Environ.*, *115*(9), 2255–2266, doi:10.1016/j.rse.2011.04.025.

D'Ortenzio, F., et al. (2010), White Book on Oceanic autonomous Platforms for Biogeochemical Studies: Instrumentation and Measure (PABIM), version 1.3. [Available at: http://www.obs-vlfr.fr/OAO/file/PABIM white book version1.3.pdf.]

Falkowski, P., D. A. Kiefer, O. S. Division, and L. Angeles (1985), Chlorophyll a fluorescence in phytoplankton: Relationship to photosynthesis and biomass, *J. Plankton Res.*, *7*(5), 715–731.

Friedrich, T., and A. Oschlies (2009), Neural network-based estimates of North Atlantic surface pCO 2 from satellite data: A methodological study, *J. Geophys. Res.*, *114*, C03020, doi:10.1029/2007JC004646.

Gordon, H. R., and W. R. McCluney (1975), Estimation of the depth of sunlight penetration in the sea for remote sensing, *Appl. Opt.*, *14*(2), 413–416, doi:10.1364/AO.14.000413.

Gross, L., S. Thiria, R. Frouin, and B. G. Mitchell (2000), Artificial neural networks for modeling the transfer function between marine reflectance and phytoplankton pigment concentration, *J. Geophys. Res.*, *105*(C2), 3483–3495, doi:10.1029/1999JC900278.

Hood, R. R., et al. (2006), Pelagic functional group modeling: Progress, challenges and prospects, *Deep Sea Res., Part II*, *53*(5–7), 459–512, doi:10.1016/j.dsr2.2006.01.025.

Hornik, K., M. Stinchcombe, and H. White (1989), Multilayer feedforward networks are universal approximators, *Neural Networks*, *2*, 359–366.

Huot, Y., M. Babin, and F. Bruyant (2013), Photosynthetic parameters in the Beaufort Sea in relation to the phytoplankton community structure, *Biogeosciences*, *10*(5), 3445–3454, doi:10.5194/bg-10-3445-2013.

Jamet, C., H. Loisel, and D. Dessailly (2012), Retrieval of the spectral diffuse attenuation coefficient K d (λ) in open and coastal ocean waters using a neural network inversion, *J. Geophys. Res.*, *117*, C10023, doi:10.1029/2012JC008076.

Johnson, K. S., L. J. Coletti, H. W. Jannasch, C. M. Sakamoto, D. D. Swift, and S. C. Riser (2013), Long-term nitrate measurements in the ocean using the in situ ultraviolet spectrophotometer: Sensor integration into the APEX profiling float, *J. Atmos. Oceanic Technol.*, *30*(8), 1854–1866, doi:10.1175/JTECH-D-12-00221.1.

Kiefer, D. A. (1973), Chlorophyll a fluorescence in marine centric diatoms: Responses of chloroplasts to light and nutrient stress, *Mar. Biol.*, *23*(1), 39–46, doi:10.1007/BF00394110.

Lavigne, H., F. D'Ortenzio, H. Claustre, and A. Poteau (2012), Towards a merged satellite and in situ fluorescence ocean chlorophyll product, *Biogeosciences*, *9*(6), 2111–2125, doi:10.5194/bg-9-2111-2012.

Le Quere, C., et al. (2005), Ecosystem dynamics based on plankton functional types for global ocean biogeochemistry models, *Global Change Biol*, *11*, 2016–2040.

Leblanc, K., et al. (2012), A global diatom database—Abundance, biovolume and biomass in the world ocean, *Earth Syst. Sci. Data*, *4*, 149–165.

Lek, S., and J. F. Guégan (1999), Artificial neural networks as a tool in ecological modelling, an introduction, *Ecol. Modell.*, *120*(2–3), 65–73, doi:10.1016/S0304-3800(99)00092-7.

Lorenzen, C. J. (1966), A method for the continuous measurement of in vivo chlorophyll concentration, *Deep Sea Res. Oceanogr. Abstr.*, *13*(2), 223–227, doi:10.1016/0011-7471(66)91102-8.

Marty, J.-C., J. Chiavérini, M.-D. Pizay, and B. Avril (2002), Seasonal and interannual dynamics of nutrients and phytoplankton pigments in the western Mediterranean Sea at the DYFAMED time-series station (1991–1999), *Deep Sea Res., Part II*, *49*(11), 1965–1985, doi:10.1016/S0967-0645(02)00022-X.

Marzban, C. (2009), Basic statistics and basic AI: Neural networks, in *Artificial Intelligence Methods in the Environmental Sciences*, edited by S. E. Haupt, A. Pasini, and C. Marzban, pp. 15–47, Springer, Netherlands.

McClain, C. R. (2009), A decade of satellite ocean color observations, *Annu. Rev. Mar. Sci.*, *1*, 19–42, doi:10.1146/annurev.marine.010908.163650.

Mignot, A., H. Claustre, F. D'Ortenzio, X. Xing, A. Poteau, and J. Ras (2011), From the shape of the vertical profile of in vivo fluorescence to chlorophyll-a concentration, *Biogeosciences*, *8*(2), 3697–3737, doi:10.5194/bgd-8-3697-2011.

Morel, A., and J.-F. Berthon (1989), Surface pigments, algal biomass profiles, and potential production of the euphotic layer: Relationships reinvestigated in view of remote-sensing applications, *Limnol. Oceanogr.*, *34*(8), 1545–1562.

Morel, A., and S. Maritorena (2001), Bio-optical properties of oceanic waters: A reappraisal, *J. Geophys. Res.*, *106*(C4), 7163–7180, doi:10.1029/2000JC000319.

Morel, A., B. Gentili, M. Chami, and J. Ras (2006), Bio-optical properties of high chlorophyll Case 1 waters and of yellow-substance-dominated Case 2 waters, *Deep Sea Res., Part I*, *53*(9), 1439–1459, doi:10.1016/j.dsr.2006.07.007.

Palacz, A. P., M. A. St. John, R. J. W. Brewin, T. Hirata, and W. W. Gregg (2013), Distribution of phytoplankton functional types in high-nitrate, low-chlorophyll waters in a new diagnostic ecological indicator model, *Biogeosciences*, *10*(11), 7553–7574, doi:10.5194/bg-10-7553-2013.

Peloquin, J., et al. (2013), The MAREDAT global database of high performance liquid chromatography marine pigment measurements, *Earth Syst. Sci. Data*, *5*(1), 109–123, doi:10.5194/essd-5-109-2013.

Raitsos, D. E., S. J. Lavender, C. D. Maravelias, J. Haralabous, A. J. Richardson, and P. C. Reid (2008), Identifying four phytoplankton functional types from space: An ecological approach, *Limnol. Oceanogr.*, *53*(2), 605–613.

Ras, J., H. Claustre, and J. Uitz (2008), Spatial variability of phytoplankton pigment distributions in the Subtropical South Pacific Ocean: Comparison between in situ and predicted data, *Biogeosciences*, *5*(2), 353–369.

Siegel, D. A., et al. (2013), Regional to global assessments of phytoplankton dynamics from the SeaWiFS mission, *Remote Sens. Environ.*, *135*, 77–91, doi:10.1016/j.rse.2013.03.025.

Telszewski, M., et al. (2009), Estimating the monthly pCO2 distribution in the north Atlantic using a self-organizing neural network, *Biogeosciences*, *6*, 1405–1421.

Uitz, J., H. Claustre, A. Morel, and S. B. Hooker (2006), Vertical distribution of phytoplankton communities in open ocean: An assessment based on surface chlorophyll, *J. Geophys. Res.*, *111*, C08005, doi:10.1029/2005JC003207.

Uitz, J., H. Claustre, F. B. Griffiths, J. Ras, N. Garcia, and V. Sandroni (2009), A phytoplankton class-specific primary production model applied to the Kerguelen Islands region (Southern Ocean), *Deep Sea Res., Part I*, *56*(4), 541–560, doi:10.1016/j.dsr.2008.11.006.

Uitz, J., H. Claustre, B. Gentili, and D. Stramski (2010), Phytoplankton class-specific primary production in the world's oceans: Seasonal and interannual variability from satellite observations, *Global Biogeochem. Cycles*, *24*, GB3016, doi:10.1029/2009GB003680.

Vidussi, F., H. Claustre, J. Bustillos-Guzmàn, C. Cailliau, and J.-C. Marty (1996), Determination of chlorophylls and carotenoids of marine phytoplankton: Separation of chlorophyll a from divinylchlorophyll a and zeaxanthin from lutein, *J. Plankton Res.*, *18*(12), 2377–2382, doi:10.1093/plankt/18.12.2377.

Vidussi, F., H. Claustre, B. B. Manca, A. Luchetta, and J.-C. Marty (2001), Phytoplankton pigment distribution in relation to upper thermocline circulation in the eastern Mediterranean Sea during winter, *J. Geophys. Res.*, *106*(C9), 19,939–19,956, doi:10.1029/1999JC000308.

Xing, X., H. Claustre, S. Blain, F. D'Ortenzio, D. Antoine, J. Ras, and C. Guinet (2012), Quenching correction for in vivo chlorophyll fluorescence acquired by autonomous platforms: A case study with instrumented elephant seals in the Kerguelen region (Southern Ocean), *Limnol. Oceanogr. Methods*, *10*, 483–495, doi:10.4319/lom.2012.10.483.